Stability and dispersibility of microplastics in experimental exposure medium and their dimensional characterization by SMLS, SAXS, Raman microscopy, and SEM

Chardel Ompala, Jean-Philippe Renault, Olivier Taché, Émeline Cournède, Stéphanie Devineau, Carine Chivas-Joly

Stability and dispersibility of microplastics in experimental exposure medium and their dimensional characterization by SMLS, SAXS, Raman microscopy, and SEM

Chardel Ompala[a,b], Jean-Philippe Renault[a] , Olivier Taché[a], Émeline Cournède[a], Stéphanie Devineau[a,c*], Carine Chivas-Joly[b*]

[a] Université Paris-Saclay, CEA, CNRS, NIMBE, 91191 Gif Sur Yvette, France

[b] Laboratoire National de métrologie et d'Essais, Nanometrology, CARMEN Platform, 29 avenue Hennequin, 78197 Trappes Cedex, France

[c] Université Paris Cité, CNRS, Unité de Biologie Fonctionnelle et Adaptative, 75013 Paris, France

Corresponding Authors

* Carine Chivas-Joly − LNE, Laboratoire National de Métrologie et d'essais, CARMEN Platform, 29, avenue Roger Hennequin, 78197 Trappes, France. Email: carine.chivas-joly@lne.fr

* Stéphanie Devineau – Université Paris-Saclay, CEA, CNRS, NIMBE, 91191 Gif Sur Yvette, France. Email: stephanie.devineau@cea.fr

Abstract

The plastic production that contributes to the global plastic reservoir presents a major challenge for society in managing plastic waste and mitigating the environmental damage of microplastic (MP) pollution. In the environment, the formation of biomolecular corona around MPs enhance the stability of MP suspensions, influencing the bioavailability and toxicity of MPs. Essential physical properties including MP stability, dispersibility, agglomeration, and dimensional size must be precisely defined and measured in complex media taking into account the formation of a protein corona. Using static multiple light scattering (SMLS), small angle X-ray scattering (SAXS), Raman microscopy, and scanning electron microscopy (SEM), we measured the particle size, density, stability, and agglomeration state of polyethylene and polypropylene MPs stabilized in aqueous suspension by BSA. SEM analysis revealed the formation of nanoplastic debris as MP suspensions aged. Our results suggest that protein adsorption favors the formation of secondary nanoplastics, potentially posing an additional threat to ecosystems. This approach provides analytical methodologies by integrating SEM, SMLS, and SAXS, for characterizing MP suspensions and highlights the effect of the protein corona on size measurements of micro/nanoplastics. Our analysis demonstrates the detectability of secondary nanoplastics by SEM, paving the way for monitoring and controlling human exposure.

Keywords

Microplastics, nanoplastics, size, dispersibility, polyethylene

1. Introduction

Global plastic production reached 500 million metric tons in 2020 and contributes to an annual plastic waste generation of 400 million metric tons and the emission of 2.2 $GtCO_2$ [1]. With a doubling of the plastic demand expected by 2050, the total plastic stocks in use, which already amount to 3.2 Gt of plastic, may increase to 7.7 Gt by 2050 if no measures are taken to reduce this trend. Due to their high stability and resistance to chemical, physical, and mechanical stresses, most plastics in use are not biodegradable. Moreover, technical solutions are currently missing to recycle widely used plastics such as polyethylene and polypropylene [2]. With the continued growth of the plastic sector and the implementation of new production units worldwide, past and ongoing plastic production pose a major challenge to our societies to manage plastic waste and to mitigate the environmental damages of plastic pollution. As the impact of plastic pollution may extend well beyond the end of plastic release in the environment, a global ‘toxicity debt’ associated with plastic pollution has emerged [3]. Lower density polymers such as polyethylene (PE) and polypropylene (PP) represent between 25 and 40% of plastic particles in surface waters, with their ultimate fate remaining unknown, whereas denser polymers such as polyesters and acrylics are more prevalent in the deep-sea and sediments, which can

represent a potential sink for these plastics [8]. Interestingly, the size of buoyant plastic particles vary in the water column, with smaller particles more susceptible to vertical transport than larger ones, a process that can be favoured by biofouling [9]. As a result, the mass metrics of plastics (in g/m^3) decrease more rapidly than the number metrics (in number/m^3) [10]. Fragmentation of plastic wastes into microplastics (MPs) by weathering has generated an estimated 15 to 55 trillion MPs in the world's oceans, putting marine organisms at risk [11]. The reduction of plastic size under the combined effects of photodegradation by UV irradiation, shear forces, hydrolysis, and biodegradation favors the long-range transportation of MPs in water and in air, leading to global MP dissemination [12] [13]. Together with polymer ageing, size reduction can favor the release of additives and the sorption of chemical contaminants by increasing the specific surface area and changing the microstructure of the particles [14]. Finally, smaller particles may cross biological barriers as evidenced by the discovery of MPs in human blood and in human placenta [15] [16]. However, there is currently no agreement on the size limits that define microplastics and nanoplastics. Indeed, the fragmentation of plastic waste into debris results in a range of particle sizes, where plastic particles with external dimensions below a certain threshold (either 100 nm or 1 µm, depending on the definition used) transition from microplastics to nanoplastics. These nanoplastics can be considered a specific category of nanomaterials.

Considering their nature and shape, MPs are defined by ECHA as solid plastic particles composed of mixtures of synthetic polymers and functional additives. The EFSA defined primary MPs as the original manufactured products, such as polystyrene pellets, and secondary MPs as particles that originate from fragmentation. A unique definition was provided for MPs based on their size as *'a heterogeneous mixture of differently shaped materials referred to as fragments, spheroids, granules, pellets, flakes or beads, in the range of 0.1 to 5,000 µm'* [17]. MPs have been recently integrated in REACH regulation [18]. In the preparation of its Microplastic Act, the European Commission suggested that the lower limit of 100 nm could be lowered to 1 nm to reduce human exposure to nanoplastics [19] [20]. However, the 100-nm size limit will probably remain in the final Act until technical and analytical solutions become available to measure MP concentration in this size range [21]. The lack of analytic means to characterize MPs may thus prevent the protection of exposed populations.

In the literature, several definitions have been proposed to conceptualize the presence of micro/nanoplastics and plastic debris in colloidal suspensions. Recently, Caldwell *et al*. [22] defined macro- (25-50 mm), meso- (5-25 mm), micro- (<5 mm), and nanoplastics (<1 µm) following the recommendations of the Joint Group of Experts on the Scientific Aspects of Marine Environmental Protection (GESAMP) [23]. While the European Commission defined nanomaterials as < 100 nm [24] [25], the OECD guidelines recently recommended to extend this size limit to < 1 µm [21].

Gigault *et al*. [26] proposed the following categories: nanoplastics (1 nm – 1 µm) with a subdivision between nanoplastics (1 – 100 nm) and submicron plastics (100 nm – 1 µm); microplastics (1 µm – 1 mm); mesoplastics (1 – 10 mm); and macroplastics (> 1 cm). An overview of the size limits used in the literature to define micro/nanoplastics and disparities between recommendations from different regulatory bodies are presented in Table 1. There is no harmonized definition of microplastics. Thus, the size limit between micro- and nanoplastics is not well defined and varies between studies.

Table 1. Disparities of the definitions of microplastics and nanoplastics proposed by the European Commission, EFSA, GESAMP, and examples from the literature adapted from Hartmann *et al*. 2019 [26] and Caldwell *et al*. 2019 [22].

	Macro-	**Meso-**	**Micro-**	**Sub-micron**	**Nano-**	**Ref.**
Browne et al. (2007)	> 5 mm		1 µm – 1 mm	n.a.	< 1 µm	[27]
Moore et al. (2008)	> 5 mm		< 5 mm			[28]
Ryan et al. (2009)	> 20 mm	2 – 20 mm	< 2 mm			[29]
Costa et al. (2010)	n.a.		< 1 mm			[30]
European Commission (2011, 2022)	n.a.				**< 100 nm**	[24] [25]
Desforges et al. (2014)	n.a.		1 µm – 5 mm			[31]
Eriksen et al. (2014)	> 200 mm	4.76 – 200 mm	0.33 – 4.76 mm	n.a.		[7]
Wagner et al. (2014)	> 5 mm	2.5 – 5 mm	20 – 500 µm	n.a.	< 20 µm	[32]
Koelmans et al. (2015)	> 5 mm		1 µm – 5 mm	n.a.	1 – 100 nm	[33]
Andrady (2015)	25 mm – 1 m	1 – 25 mm	1 – 100 µm	n.a.	< 1 µm	[34]
Ivleva et al. (2017)	> 25 mm	5 – 25 mm	1 – 5 µm	0.1 – 1 µm	< 100 nm	[35]
Hernandez et al. (2019)	n.a.		1 – 200 µm	< 1 µm	< 100 nm	[20]
EFSA (2016)	n.a.		**0.1 µm – 5 mm**	n.a.	**1 – 100 nm**	[17]
Gigault et al. (2018)	> 10 mm	1 – 10 mm	1 µm – 1 mm	1 – 100 µm	1 – 100 nm	[26]
GESAMP (2019)	**25 mm – 1 m**	**5 – 25 mm**	**< 5 mm**	n.a.	**< 1 µm**	[23]
Caldwell et al. (2019)	> 20 mm	5 – 20 mm	1 µm – 5 mm	n.a.	n.a.	[22]
OECD (2022)	n.a.				**< 1 µm**	[21]

Toxicological studies require model or standard materials that are both reproducible and easy to manipulate in order to investigate the effects of defined chemical composition, size, shape, and concentration on the biological response at a molecular, cellular or organism level. Standardized test nanomaterials in the form of stabilized colloidal suspensions with well-defined sizes provided by the Joint Research Centre (JRC) have been extensively used in the field of nanotoxicology for toxicity studies, interlaboratory comparisons, calibration of analytical devices, and development of bioassays

[36]. However, no such reference materials exist for MP suspensions, with the exception of functionalized polystyrene spheres.

The stabilization of MPs is not straightforward due to the high hydrophobicity of synthetic polymers such as PE and PP and their low density resulting in fast or instant creaming of the particles from the suspension. One common method consists in exposing particles to proteins, such as bovine serum albumin (BSA), which results in the formation of a stabilizing protein corona. The exceptional coating properties of BSA with respect to PE and PP MPs for the preparation of MP suspensions has been demonstrated [37]. In the environment, a similar phenomenon spontaneously occurs in the presence of biomolecules resulting in the formation of an eco-corona [38]. This biomolecular corona enhances the transport of MPs by changing their mobility [39] and changes their bioavailability, uptake, and toxicity with respect to living organisms [40]. However, the question of the state and the fate of MPs in such dispersions is far from being understood. Key physical properties – MP stability, dispersibility, agglomeration, and dimensional size – must be defined and measured in complex media, such as the ones used in toxicological studies, by taking into account the formation of both naturally or intentionally developed corona. This knowledge will help to understand the behavior of micro/nanoplastics in suspension, provide adapted analytical methods to characterize MPs and develop reference materials for toxicity studies.

The stabilization of MPs in suspension by a biomolecular corona is essential to perform the dimensional characterization of MPs and to reproduce real-life scenarios of exposure. The dimensional measurement of particles in suspension is difficult if stability and dispersibility are not ensured. The main objectives of this study are to complete the dimensional characterization of MPs in suspension and to improve the current comprehension of the behavior and impact of the corona on size measurements of micro/nanoplastics. Our specific aims were as follows:

(i) to examine the role of the corona on the stability, dispersibility, and dimensional size of MPs;

(ii) to elucidate the influence of the corona on the fate of micro/nanoplastics and the possible release of secondary nanoplastics;

(iii) to explore the dimensional size analysis of micro/nanoplastics in suspension.

To better understand the interactive effects and mechanisms between the corona and MPs, we focused our study on two polyolefin MPs, polyethylene and polypropylene, which are widely present in MP pollution, and a model protein, BSA, which is compatible with toxicity studies. The dimensional size analysis of MPs in freshly prepared suspension was compared by SEM, SMLS, SAXS, and Raman microscopy as a function of BSA concentration. The MP suspensions were then aged for 7 days in shelf storage conditions to evaluate the stability, dispersibility, and size evolution of the MPs over time.

2. Experimental

The combination of existing methods and the development of novel methodologies are necessary to fully characterize micro- and nano-plastic suspensions. PE and PP MPs with a corona formed by BSA were characterized by SMLS, SAXS, SEM, Raman microscopy, and zetametry.

2.1. Materials

Polyethylene and polypropylene MPs are widely present in the environment [8] and as contaminants in tap water [42]. PE and PP MPs were purchased from Clariant (Germany) in powder form (Ceridust 3610, Ceridust 60050M). The characterization of PE and PP MPs in powder form is provided in Table 2 [37]. Densities of 0.97 and 0.90 $g.cm^{-3}$ for PE and PP respectively were indicated by the manufacturer. No surface contaminants were detected by XPS [37].

Table 2. Physical properties of PE and PP microplastics in powder form [37]

Physical properties	**Technique**	**PE Ceridust 3610**	**PP Ceridust 60050M**
Diameter (µm)	Optical microscopy	4.2	10.0
Surface specific area (m^2/g)	SAXS	2.5	1.1
Number of crystalline phases	Raman microscopy	3	1

BSA was chosen as a model protein to stabilize PE and PP MPs in aqueous suspensions based on its high affinity for MPs and its good surfactant properties [37] [43]. The isoelectric point of BSA is around 4.8 and its molecular mass is 66,450 Da. BSA has been widely used for the stabilization of nanomaterials in the field of nanotoxicology [44], and is a good candidate for the preparation of reference test materials for the study of MP toxicity. Lyophilized BSA was purchased from Sigma-Aldrich (France) (reference A7030), dissolved in milliQ water, dialyzed using a porous membrane with a cut off of 3.5 kDa (Spectra/Por) at 4°C, and centrifuged at 15,000 g for 5 minutes. BSA solutions were freshly prepared before use, and the protein concentration was checked by UV spectroscopy.

2.2. Sample preparation

2.2.1. Dispersion protocol and formation of a protein corona

The dispersion protocol of MPs in BSA solutions adapted from [37] is presented in Fig. 1. PE and PP in powder form were weighed and dispersed in a BSA solution to obtain final MP suspensions with a particle concentration of 10 g/L and BSA concentrations of 0.03, 0.09, 0.15, and 0.3 g/L. The colloidal suspensions were mixed on a rotating wheel at 3 rpm at 20°C for 3 days.

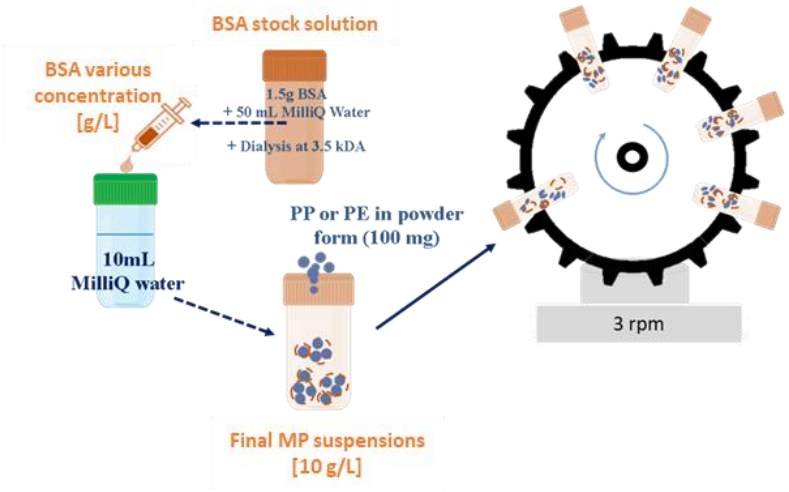

Fig. 1. Schematic of the dispersion protocol of polyethylene and polypropylene MPs in BSA solutions, adapted from [37]. The final concentration of MPs was 10 g/L and the total concentration of BSA varied between 0.03 and 0.3 g/L to form a complete protein corona on PE and PP MPs with increasing concentrations of free BSA in solution.

The adsorption isotherms of BSA on PE and PP microplastics adapted from [37] are shown in Fig. 2 and Fig. S1. Note that the available surface is higher for PE than for PP MPs at a fixed MP mass concentration of 10 g/L (Table 2). The minimum concentration of BSA (0.03 g/L) was chosen so that a quasi-complete corona was formed on both PE and PP particles with a minimal amount of free BSA in solution. Higher BSA concentrations (0.09, 0.15, and 0.3 g/L) were chosen to provide an excess of free BSA. For PE MPs, there was a 1-fold excess for a total BSA concentration of 0.09 g/L (40 mg adsorbed + 50 mg free in solution), a 3-fold excess at 0.15 g/L (40 mg adsorbed + 110 mg in solution), and a 6-fold excess at 0.3 g/L (40 mg adsorbed + 260 mg in solution).

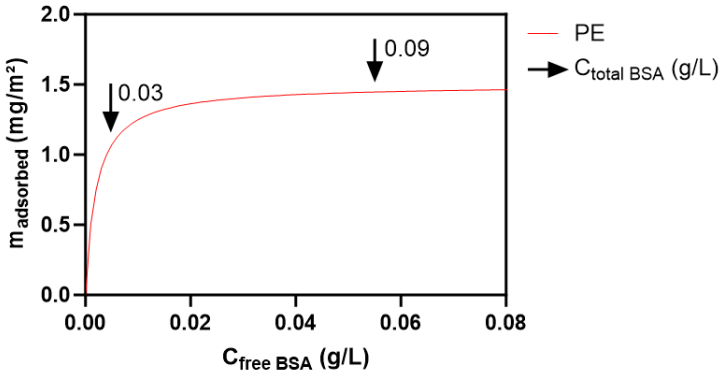

Fig. 2. Adsorption isotherms of BSA on PE MPs represented by the Langmuir model, adapted from [37]. The corresponding concentrations of total BSA are shown by arrows for C(BSA) = 0.03 g/L and C(BSA) = 0.09 g/L.

2.2.2. Ageing of MPs suspensions

The use of a purified protein such as BSA allowed us to follow the evolution of MP suspensions over longer periods. The PE and PP MP suspensions prepared as described above were aged for 7 days in shelf-storage condition at 20°C without agitation to monitor the release of secondary nanoplastics in the suspension. The aged suspensions were gently mixed for 10 min on a rotating wheel at 3 rpm before analysis by SMLS, SEM, and Raman microscopy. No bacterial contamination of MPs or MP suspensions was observed. The analysis was performed for 4 different BSA concentrations. The same suspensions were analyzed before and after ageing.

2.3. Characterization techniques and measurands

In this study, colloidal stability was evaluated by zeta potential and SMLS. The zeta potential of MP suspensions was measured as a function of BSA concentration. The SMLS technique allows the measurement of the Turbiscan Stability Index (TSI) and the creaming rate of MP dispersions, which is a predictive indicator of colloidal stability. Size can be characterized by measuring the initial mean size of particle by SMLS and SEM. Each technique has its own dimensional measurand (d_{SMLS} (t=0) and d_{SEM} respectively) and thus brings complementary information about MP dispersion state, whereas Raman provides a molecular fingerprint spectrum based on the polarizability of chemical bonds. Raman microscopy can also provide *in situ* information on the constituent size of MPs in agglomerates from colloidal suspensions. The Stokes diameter (d_{Stokes}) corresponding to the equivalent diameter from the particle creaming rate also depends on the particle density, which was experimentally determined by SAXS.

The definitions of the main terms based on ISO standards are provided here for clarity [41]. Stability is defined as the evolution of the physico-chemical state of MPs over time, whereas dispersibility represents the property of MPs to be uniformly distributed in a specific medium. An aggregate is defined as an assemblage of particles in a rigid structure, usually formed in an irreversible process by covalent bonds. By contrast, an agglomerate is a 'loosely coherent assembly of particles (or aggregates) held together by weak physical interactions and with a total surface area virtually equal to the sum of the surface areas of the constituent particles' [41].

2.3.1. Zeta Potential and pH

The zeta potential of MP suspensions was measured as a function of BSA concentration on a Malvern Zetasizer at 25°C in water. Three measurements were done for each suspension. The zeta potential was calculated using the Smoluchowski method. Data correspond to the mean and the standard deviation of 3 independent series (n = 3). The pH of the suspensions was measured at room temperature (20°). The pH value corresponds to the mean ± standard deviation of 3 independent replicates.

2.3.2. Static multiple light scattering (SMLS)

SMLS is a technique based on static light scattering dedicated to the measurement of the particle mean size in the initial conditions, the creaming rate, and the macroscopic stability of colloidal suspensions [45]. MP colloidal suspensions were analyzed by SMLS with a Turbiscan® Lab (Formulaction, France).

Monochromatic infrared light of wavelength λ = 880 nm propagated in the MP suspension contained in a cylindrical glass tube. Two detectors collected the light scattered by the medium. The first one is placed at an angle of 0° to the source (i.e., opposite to the incident wave) to collect light transmitted by the medium. The other detector is placed at an angle of 135° to collect the backscattered signal (BS). The highest intensity was measured for backscattered light with both PE and PP suspensions. The first scan measured at t = 0 s was used to evaluate the mean particle size by volume, d_{SMLS} (t = 0), assuming the particle concentration is homogeneous in the suspension.

When particles rose towards the surface, a clarification zone formed at the bottom of the sample favoring the onset of a creaming peak. The peak width as a function of time is proportional to the creaming speed of MPs. It is thus possible to calculate the Stokes diameter, d_{Stokes} (t ≠ 0), corresponding to a hydrodynamic diameter, from the particle creaming velocity. In addition to particle diameters, a stability index called TSI (Turbiscan Stability Index) was evaluated from the differences in backscattered intensity at a given time (eq. 1):

$$TSI(\mathrm{t}) = \frac{1}{N_z}\sum_{t_i=1}^{t_{max}}\sum_{z_i=z_{min}}^{z_{max}}|BST(t_i, z_i) - BST(t_{i-1}, z_i)| \quad (1)$$

with t_{max} the time at which the TSI is calculated and BST the considered signal. Consequently, when the TSI is high, the colloidal suspension tends to be unstable. Each measurement is the average of 3 replicates. The mean values of TSI, d_{SMLS}, and d_{Stokes} correspond to the mean of 3 independent series (n = 3), except for aged suspensions (n = 1).

2.3.3. Scanning electron microscopy (SEM)

7.5 µL of BSA-PE or BSA-PP suspensions was deposited on a silicon substrate using a LabSpin 6 spin coater system (SUSS MicroTec) (Fig. 3). To improve the deposit of negatively charged particles, the substrate was pre-coated with positively-charged polylysine (PLL) (Serva Electrophoresis, Thermo Fischer scientific). The effect of PLL coating on the quality of MP deposits was evaluated by comparing the SEM images of the same samples, with and without PLL coating of the Si wafer. MPs were imaged using an SEM Zeiss ULTRA-Plus equipped with a Field Emission Gun (FEG) source and in-Lens SE detector. The images were measured using secondary electrons collected by the In-Lens detector at 3 kV at a 3.0 mm working distance. The charge compensator system was used to blow nitrogen gas near the samples and neutralize negative charges. The diameter equivalent to the projected particle surface was measured using Platypus™ software [46] assuming that particles were spherical. We measured MP size by manually adjusting an ellipse on the entire particle using Platypus™ software (Fig. S2). Then the particle edge and corresponding area inside the edge were

automatically calculated. The primary size measurement of MPs was done on a stack of 10 to 15 SEM images to measure a minimum number of 300 particles. The expansion of the distribution σ was measured in triplicate on MP suspensions with a 95% confidence interval.

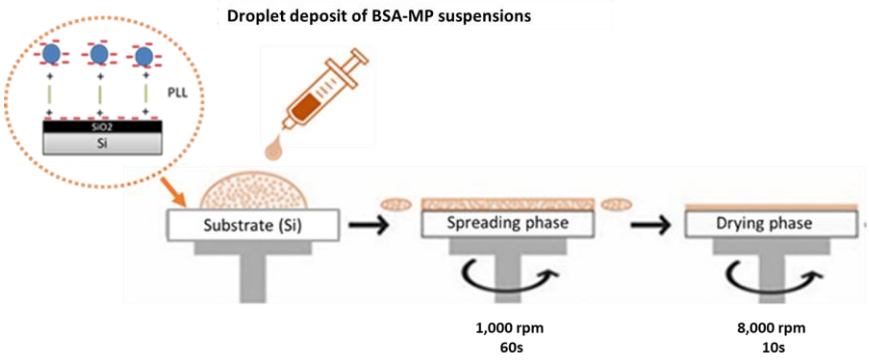

Fig. 3. Schematic of the deposition of micro- and nano-plastic suspensions on silicon wafers by spin-coating for SEM analysis after pre-coating by PLL.

According to our observations, PLL functionalization promoted immediate adhesion of nanoplastics (< 1 µm) to the silicon wafer.

The measurand used for the SEM corresponds to an area-equivalent diameter. For particles with irregular shapes, an equivalent diameter was calculated from a projected surface area assuming that the particles are spherical. The average diameter, D, corresponding to the average of area-equivalent diameters, and the population number-weighted size distribution were determined. The repeatability uncertainties related to the measurements (u_R) correspond to the standard deviation calculated on the average diameters of 3 independent replicates.

2.3.4. Raman microscopy

The agglomeration state of MP suspensions was investigated *in situ* by confocal Raman microscopy. 10 µL of PE and PP BSA-MPs suspensions was deposited between two fused silica substrates (ESCO Optics, UK) and held in an AttoFluor Cell Chamber (Invitrogen, France) to limit particle motion during imaging. Raman images were acquired on a WITec alpha300 RA Raman microscope (Oxford Instruments) with a Zeiss 100x oil immersion objective (NA 1.3) using an excitation wavelength of 532 nm and a grating of 600 g/mm. Exposure time was set to 10 ms and laser power to 10 mW for a spatial step of 0.3 µm. Raman spectra were treated using WITec Program 5 software to remove cosmic rays and subtract baseline. Raman images were reconstructed using the True Component Analysis toolbox.

The Raman images of PE were further segmented to measure the size of the constituent particles in the agglomerates using the SAM segmentation model developed by META [47]. This approach allowed good segmentation of the Raman images without pre-treatment and preliminary training of the model, taking advantage of META SA-1B dataset.

The same experimental setup was used for Raman imaging and for recording movies of MP suspensions with a 100x oil immersion objective and white light illumination in reflection mode. Movies were recorded at 25 frames per second for 10 s. Bright field images were analyzed with Fiji software (version 1.53t) [48].

2.3.5. Small angle X-ray scattering (SAXS)

The particle density of PE and PP MPs were measured in suspension by SAXS using a Xeuss 3.0 instrument (Xenocs, France) equipped with a copper source and an automated sampler (BioCube with robotic arm). Possible limitations in SAXS analysis of MP suspensions are the creaming of the particles during measurement, MP loss by adhesion to surfaces, and MP agglomeration. To avoid these effects, we used automated sampling and we chose MP suspensions that contained an excess of BSA to favor passivation of the tubing and surfaces. MP suspensions were analyzed under vacuum in glass capillary tubes (d = 1.5 mm) with a sample-to-detector distance of 1.8 m and a counting time of 1,800 s. Data correspond to the average of 3 measurements. Data were corrected for the capillary thickness and the water signal was subtracted. The density of PE MPs was calculated using the plateau value of the Porod limits assuming that particles have a smooth surface.

The quantity of interfaces in the suspension were measured by the Porod's limit (eq. 2) [49]:

$$\lim_{q\to\infty} Iq^4 = 2\pi \times \Delta\rho^2 \times \sum_{Porod} VSSA \quad (2)$$

where $\lim_{q\to\infty} Iq^4$ is the Porod's limit in $cm^{-1}.Å^{-4}$, I(q) the intensity of scattered light, $\Delta\rho^2$ the contrast in scattering length density (SLD) which depends on the density of the particle ρ_{MP} and the density of the solvant ρ_{H2O}, and $\sum_{Porod} VSSA$ the amount of interfaces per volume unit of dispersion in cm^{-1}. No difference in SLD was observed between BSA solutions and water in these conditions.

$\sum_{Porod} VSSA$ is related to the amount of interface per mass of particle $\sum_{Porod} SSA$ in $m^2.g^{-1}$ (eq. 3) :

$$\sum_{Porod} VSSA = \sum_{Porod} SSA \times C \quad (3)$$

where C is the mass concentration of particle in solution.

$\sum_{Porod} SSA$ in $m^2.g^{-1}$ was calculated as the ratio of the surface S of a particle by its mass m_{MP} (expressed as the product of its volume V and density ρ_{MP}). S and V are then expressed as a function of the particle diameter d_{Porod} to obtain eq. 4:

$$\sum_{Porod} SSA = \frac{S}{\rho_{MP} \times V} = \frac{6}{\rho_{MP} \times d_{Porod}} \quad (4)$$

2.4. Statistical analysis

SEM, SMLS and RAMAN data are presented as mean ± standard deviation of 3 replicates. Statistical analysis was performed with Prism GraphPad Software (v.10.0). Data were tested for normality with a Shapiro-Wilk test and analyzed by multiple two-way ANOVA with a post-hoc Tukey test. P-values < 0.05 were considered statistically significant.

The repeatability uncertainties of SEM measurements were determined following the methodology developed by Bouzakher-Ghomrasni et al [50]. Briefly, the estimation of the law parameters that best fits the SEM data was carried out using R-Studio software. The size distribution was estimated using the Maximum-Likelihood estimation statistical method. Prior to the calculation, a choice has to be made regarding the theoretical probability distribution that is suitable to represent the size distribution. Four theoretical models: Gaussian, Lognormal, Gaussian mixture, and Lognormal mixture, were used to draw the histograms. The probability density function (PFD) of the 4 models was determined for the measured sizes of the single particles. To discriminate between the 4 models, we used the Akaike Information Criteria (AIC) and the Bayesian Information Criteria (BIC). The best model is the one that has a minimum AIC and/or BIC, with the BIC criterion preferred in case of conflict. Lognormal distribution was selected for the size measurement of MPs by SEM based on this criteria.

3. Results

3.1. Stability of MP suspensions with a BSA corona

PE and PP MPs were stabilized in aqueous solution by the formation of a BSA protein corona, following previous work by Schvartz *et al*. [37]. The formation of a protein corona is necessary to obtain MP suspensions, since no particles were detected in solution without protein. First, the stability of MP dispersions in BSA solutions was assessed by SMLS to evaluate the effect of the concentration of free BSA in solution. The Turbiscan Stability Index (TSI), which provides macroscopic information on the stability of colloidal suspensions, was measured after 12 h without mixing (Fig. 4a). No significant change of the TSI was observed by increasing the concentration of BSA from 0.03 to 0.3 g/L corresponding to a complete protein corona with no excess to a 6-fold excess of free BSA, respectively (Fig. 2, see 2.2.1). A similar effect was observed for PP MP suspensions (Fig. S3). The creaming rate *Vc* of PE MPs did not vary significantly with BSA concentration, with values between 2.2 and 2.6 mm/h (Fig. 4b). PE MP suspensions with and without an excess of free BSA were aged for 7 days (shelf storage at 20°C) to investigate the release of secondary particles and/or aggregation over time. After ageing in shelf-storage conditions for 7 days and gentle mixing for 10 min, the TSI and creaming rate of the colloidal suspensions were measured again. No increase in TSI and *Vc* was observed, confirming the good stabilization of PE MPs by BSA.

While the increase in free BSA had no impact on the stability of PE and PP MPs, a higher TSI (TSI > 32) and creaming rate (*Vc* > 10 mm/h) were observed for PP compared to PE MPs (Fig. S3). The fast creaming of PP MPs was illustrated by pictures taken after 1 and 3 h resting in all the conditions tested (Fig. S4). The lower stability of PP MPs suspensions over time despite the formation of a complete protein corona could be explained by the larger size of PP particles compared to PE, as reported by Schvartz *et al*. [37]. We note that in the case of PP MPs, there was a 9-fold excess of free BSA at a concentration of 0.3 g/L (Fig. S1).

The surface charge of MPs with a BSA corona was evaluated by zeta potential measurement. PE MPs were negatively charged (ζ = -35.9 ± 1.5 mV) with no significant change with increasing BSA concentration (Fig. S5). A negative zeta potential was also measured for PP MPs covered by negatively-charged BSA (ζ = -48.4 ± 1.4 mV). The pH of the suspensions did not change significantly with BSA concentration (pH = 7.4 ± 0.1) (Table S1). This is in agreement with the stabilization of hydrophobic MPs by adsorbed BSA that acts as a charged surfactant [43] and improves the hydrophilicity of the particles.

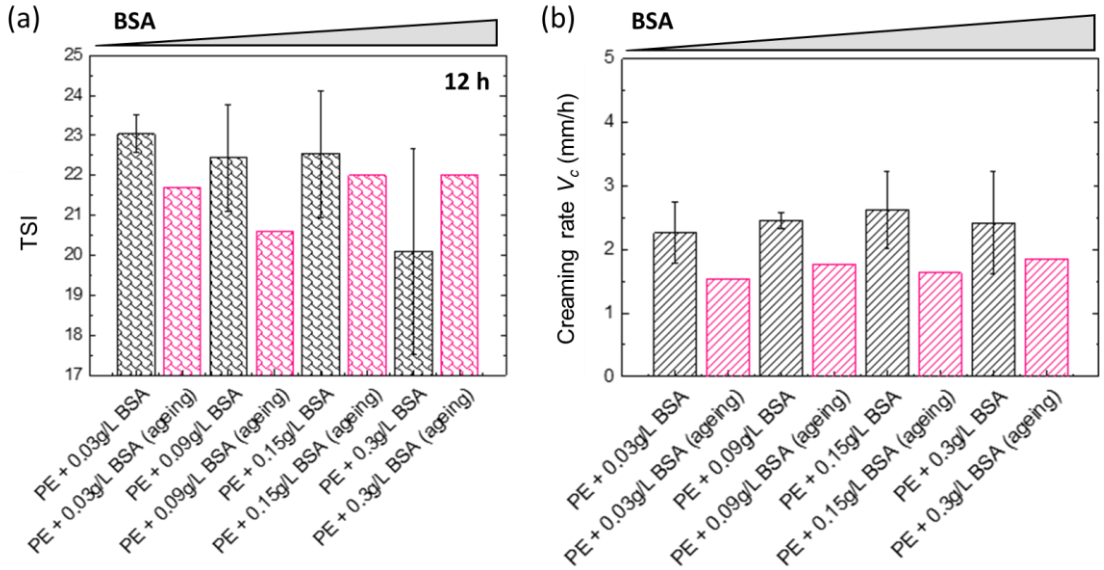

Fig. 4. Stability of PE MP suspensions with a protein corona measured by SMLS as a function of BSA concentration. (a) TSI (Turbiscan Stability Index) measured at 12 h, and (b) Creaming rate V_c (mm/h) of fresh MP suspensions (grey bars) and MP suspensions aged for 7 days (pink bars). C(MP) = 10 g/L. Values correspond to the mean and standard deviations of 3 independent series (n = 3), except for the aged series (n = 1).

3.2. Determination of MP dimensional size and dispersibility by SEM

The utilization of SEM for characterizing nanomaterials in environmental or biological samples has become a standard practice in the field of nanotoxicology [51] [52]. However, this technique is still seldom used efficiently for micro- and nanoplastics as it requires specific operating conditions to

prevent any fusion or bubbling of the polymer under the electron beam. In this study, we recorded high quality SEM images of MPs without carbon coating by using a charge compensator system. The SEM images of PE MPs deposited on PLL-treated and untreated Si wafers as a function of the concentration of BSA in the suspension are shown in Fig. 5.

The projected diameter of primary particles, either isolated or in agglomerates/aggregates, was measured after segmentation using PLATYPUS software, as illustrated in Fig. S2. The mean diameter of PE MPs in suspension, d_{SEM} = 4.7 ± 0.6 µm for condition without excess BSA in solution (C_{BSA} = 0.03 g/L) (Fig. 6a) is in good agreement with the diameter of 4.2 µm measured on PE in powder form (Table 2) [37], confirming that drying of MPs suspensions on a Si substrate did not alter the size measurement. Good agreement was also obtained for PP MP suspensions with a mean diameter of the primary particles d_{SEM} = 11 ± 2 µm compared to a diameter of 10 µm in powder form (Fig. S6-S7).

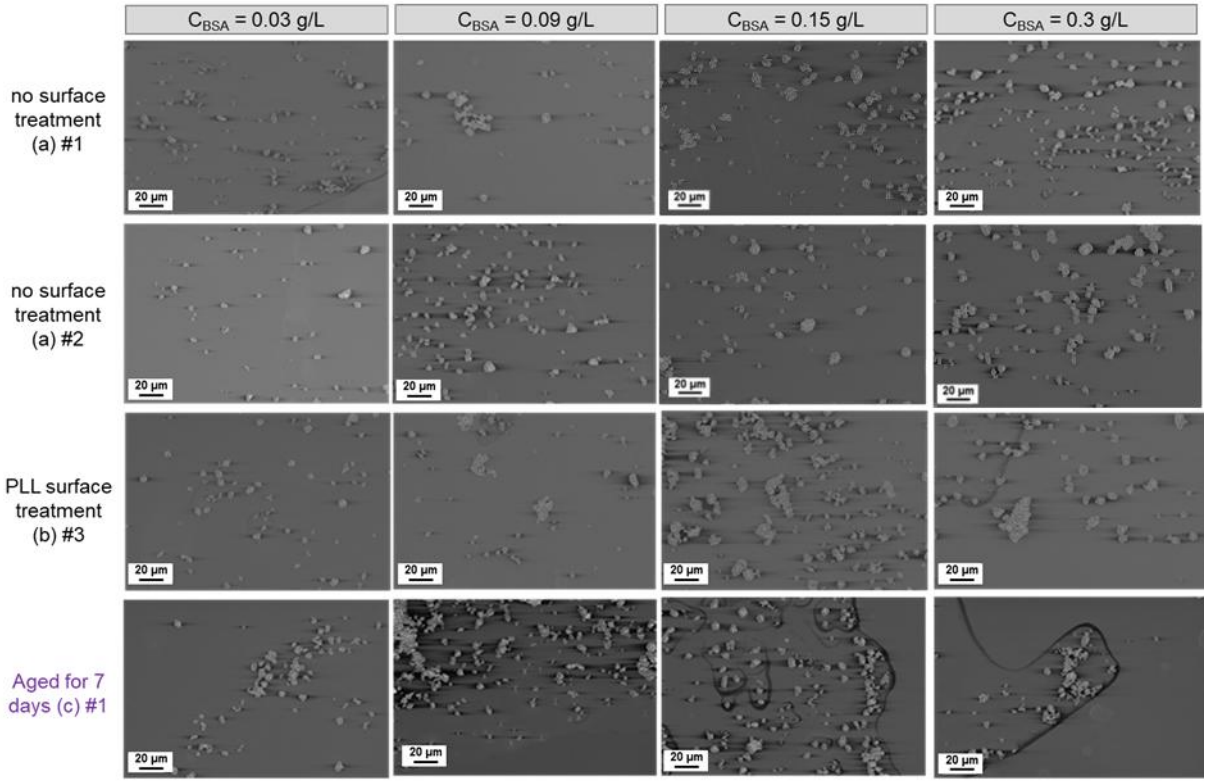

Fig. 5. SEM images of PE MPs deposited on silicon wafers as a function of BSA concentration in the suspension. The conditions presented are (a) no surface treatment, (b) PLL-coated Si, (c) ageing of PE MPs suspension for 7 days. The series numbers are indicated. Scale bar 20 µm.

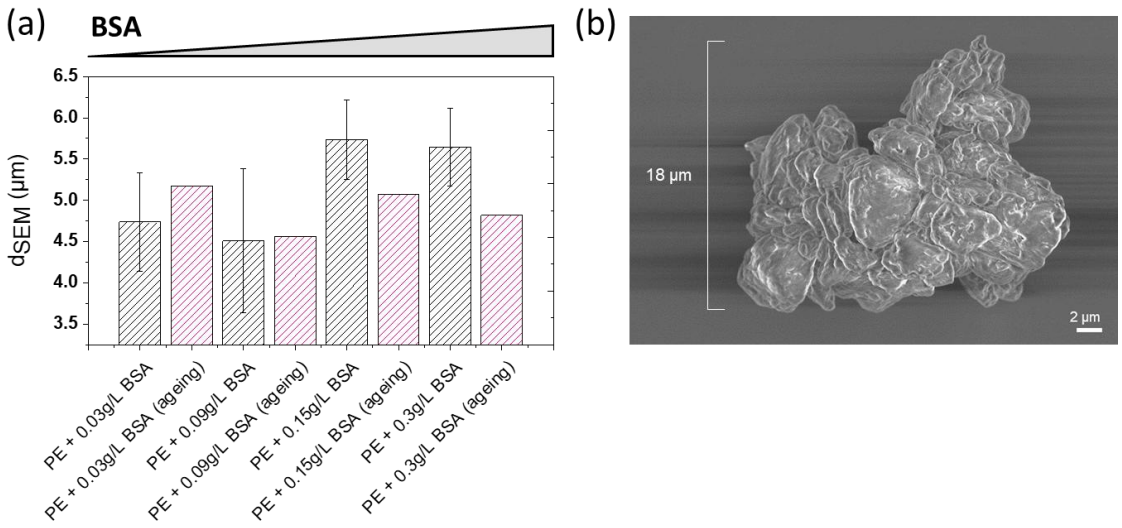

Fig. 6. Dimensional size of primary particles of PE MPs with a BSA corona measured by SEM. (a) Average SEM diameter as a function of BSA concentration for fresh suspensions (grey) and suspensions aged for 7 days (pink). n = 3 for fresh MPs suspensions, n = 1 for aged MPs suspensions. (b) Representative image of an agglomerate/aggregate of PE MPs (C_{BSA} = 0.09 g/L). Scale bar 2 µm.

The dispersibility of MPs can be qualitatively estimated by the homogeneity and the surface density of the isolated particles of the deposits, reflecting the propensity of primary particles to remain dispersed and to preserve their original size in suspension. To estimate the homogeneity of the deposit, the expansion of the distribution σ was determined for each MP suspension. The smaller the expansion of the distribution, the narrower is the particle size distribution. σ was estimated with a 95% confidence interval to 0.3 and 0.4 for PE and PP MPs, respectively. For σ > 0.3, the equivalent diameter becomes larger due to particle agglomeration/aggregation in suspension. To illustrate this effect, a representative SEM image of an aggregate/agglomerate of PE MPs is shown in Fig. 6b. However, few large objects were observed in all the conditions tested. The number of aggregates/agglomerates was estimated to less than 5% of the total number of objects observed in SEM deposits. The characterization of the aggregates/agglomerates by SMLS and Raman imaging will be presented in the next sections.

Additionally, as same-charge particles and substrates may impact particle deposition, we tested the surface treatment of Si wafers by positively-charged PLL before spin-coating of negatively-charged MPs suspensions (Fig. 3). No significant change of the dispersibility or primary particle diameter was observed with and without PLL-surface treatment, suggesting that this protocol was not necessary for the deposition of MPs with a BSA corona in the micron-size range. Besides, no significant difference in d_{SEM} was observed for PE and PP MPs as a function of BSA concentration. Overall, the MP diameter and the dispersibility of PE and PP MPs in suspension appeared unchanged with the increase of BSA concentrations.

3.3. Determination of MP density by SAXS

The density of MPs is an important factor for the calculation of the Stokes diameter by SMLS, which is calculated from the particle creaming velocity [45]. We developed a methodology based on SAXS to precisely determine the MP density in suspension. The advantages of this approach are to take into account the biomolecular corona and to provide a measurement of the density with a better accuracy compared to other techniques. The density of PP MPs could not be measured by SAXS due to the fast creaming and lower stability of the suspensions.

Porod's limit depends on the intensity of scattered light I(q), the amount of interfaces, and the contrast in scattering length density (SLD) (eq. 2). The SLD depends on the electron density, hence on the atomic composition and on the material density. The atomic composition of PE MPs is known, but not the particle density. The density of the particles can be calculated using the plateau value of the Porod's limits, as shown by Garcia-Diez et al [53, 54]. The particle diameter d_{Porod} can be directly associated to the measured Porod's limit $\lim_{q\to\infty} Iq^4$ and particle density ρ_{MP} in $g.cm^{-3}$ (eq. 3, eq. 4) (see Methods section for detailed calculation). The calculated particle Porod diameter d_{Porod} as a function of the particle density ρ_{MP} for PE MPs was plotted for the Porod's limit values of 4.6×10^{-10} $cm^{-1}.A^{-4}$ measured for C(BSA) = 0.06 g/L (Fig. 7). We can notice that our approach is simpler than the one described in the literature, as the particle diameter was determined by SEM independently from the SAXS measurements. The uncertainty on the density is given here by the minimum and maximum Porod's limits values of 3.6×10^{-10} $cm^{-1}.A^{-4}$ and 5.9×10^{-10} $cm^{-1}.A^{-4}$ respectively measured on 3 independent replicates. We chose MP suspensions that contained an excess of BSA to favor the passivation of the tubing by BSA during automated sampling and to limit MP loss and/or aggregation. This is shown by the deviation observed at C(BSA) = 0.03 g/L, while good consistency was observed at higher BSA concentrations (Fig. S8). d_{Porod} was assimilated to d_{SEM} as both techniques are sensitive to the electron density of the material. Using d_{SEM} in each condition and the observation that the particles are relatively smooth based on SEM imaging of the surface (Fig. S9), we could deduce a density range for PE MPs in suspension corresponding to an average density $\rho_{MP} = 0.90 \pm 0.01$. The particle density measured by SAXS significantly differ from the value of 0.97 $g.cm^{-3}$ given by the manufacturer for the HDPE source material (without indication on the method used). Our SAXS data indicate that the density of PE particles is closer to 0.90 $g.cm^{-3}$, suggesting that the MPs are composed of LDPE rather than HDPE. The difference between our results and the provider's ones may be due to the processing of an initially high density raw material into microparticles that may decrease the particle density, possibly through the increase of the amorphous or low cristallinity phases identified by Raman microscopy [37].

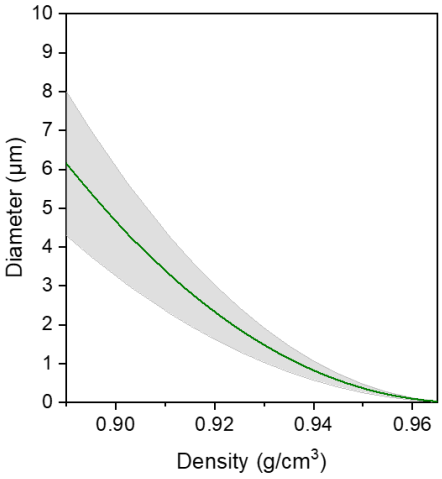

Fig. 7. Calculated MP diameter as a function of MP density determined from the Porod's limits measured by SAXS for PE MPs suspensions with C(BSA) = 0.06 g/L. The average of 3 independent replicates is shown (green line). Minimum and maximum values of Porod's limits are represented by the grey area.

A difference of < 1% of the density was obtained between C(BSA) = 0.06 g/L and C(BSA) = 0.3 g/L (Fig. S8). This difference can be explained by the uncertainty in the concentration of MP suspensions used to calculate the amount of interface. Indeed, the mass of a complete BSA corona represents only 0.2% (0.01 pg per particle) and 0.05% (0.3 pg per particles) of the mass of PE and PP particles, respectively. The effect of the BSA corona on the measurement of MP density in suspension is thus negligible. Note that this measurement cannot be performed without a protein corona to stabilize MPs in aqueous suspension. By combining SEM and SAXS, this methodology allows the measurement of the density of MPs in suspension with a sensitivity that is difficult to achieve by other techniques.

3.4. Determination of MP dimensional size and Stokes diameter by SMLS

Two diameters can be deduced from the SMLS measurements: d_{SMLS} (t = 0) and d_{Stokes} (t ≠ 0) (Fig. 8, Fig. S10). d_{SMLS} was measured at the initial time point from the light scattering properties of the particle suspension, while d_{Stokes} was measured during the evolution of the dispersion with time based on its hydrodynamic properties [45]. The mean diameters of PE MPs measured *in situ* by SMLS and *ex situ* by SEM were d_{SMLS} = 3.6 ± 0.6 µm and d_{SEM} = 4.7 ± 0.6 µm for C(BSA) = 0.03 g/L. The mean diameters of PP MPs were d_{SMLS} = 10.1 ± 1.3 µm and d_{SEM} = 10.9 ± 2.2 µm for the same conditions. The difference between d_{SEM} and d_{SMLS} may arise from the anisotropy of the particles as d_{SEM} is related to a projected surface whereas d_{SMLS} is associated with volumetric information. No significant difference in d_{SMLS} was observed with different concentrations of free BSA in solution. Moreover, no effect of ageing was observed in any of the conditions tested (Fig. 8a), confirming the good stability of PE MP suspensions after storage and re-suspension.

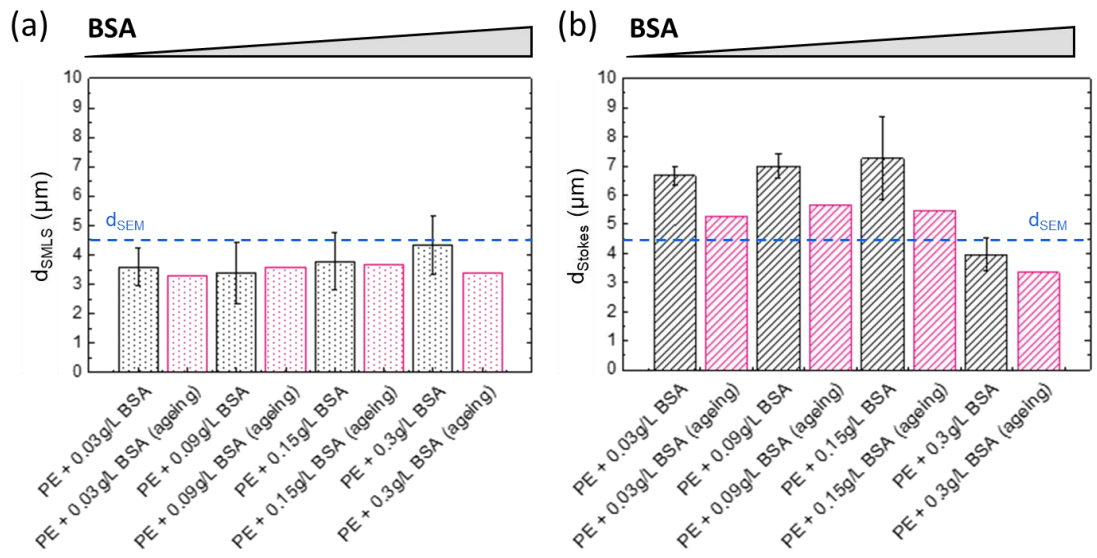

Fig. 8. *In situ* dimensional size analysis of PE MP suspensions by SMLS as a function of BSA concentration. (a) Average SMLS diameter measured at t = 0 and (b) average Stokes diameter measured at t ≠ 0 for fresh suspensions (grey) and suspensions aged for 7 days (pink). n = 3 for fresh MP suspensions, n = 1 for aged MPs suspensions. The average SEM diameter measured for C(BSA) = 0.03 g/L is reported on the dotted blue line.

The Stokes diameter of PE MPs, d_{Stokes} = 6.7 ± 0.3 µm for C(BSA) = 0.03 g/L, is not significantly different from d_{SMLS} and d_{SEM}, except for the highest concentrations of BSA (Fig. 8b). This result suggests that agglomeration or aggregation took place in the suspension during the experimental time of 24 hours. Interestingly, this effect did not hamper the stability of the dispersion as evidenced by the low creaming rate, suggesting that MP density is the main determinant of particle creaming. In the case of PP MPs, d_{Stokes} was equivalent to d_{SEM} and d_{SMLS}. However, fast creaming suggests that the largest particles have been removed from the suspension by creaming during the experimental time (Fig. S10b). Note that stability, dispersibility, and the average diameter of PE MPs did not change after 7 days of ageing in shelf-storage conditions.

3.5. *In situ* analysis of particle-particle interactions by Raman microscopy

To further investigate the formation and nature of MP agglomerates or aggregates in the suspensions, *in situ* observation of particle assemblages with sizes > 15 µm was conducted by Raman microscopy. Large objects were observed in PE suspensions only, while only single particles were detected in PP suspensions in the same experimental conditions. The Raman images revealed a high degree of hydration with a layer of water separating loosely bound particles that assembled in dynamic agglomerates (Fig. 9a). The deconvoluted Raman spectra are shown in Fig. S11. The same organization of hydrated agglomerates was observed for all BSA concentrations (Fig. S12). The horizontal stray lines visible on some Raman images are due to the binding or detachment of particles to/from the agglomerate during scanning. This was confirmed by the observation of highly dynamic

particle-particle interactions by video-microscopy in reflection mode (Movies S1-S4). Overall, these results show that PE MPs do not form tight and covalently-bound aggregates, but highly dynamic and hydrated agglomerates that can appear and disappear through transient particle-particle interactions inside the suspension.

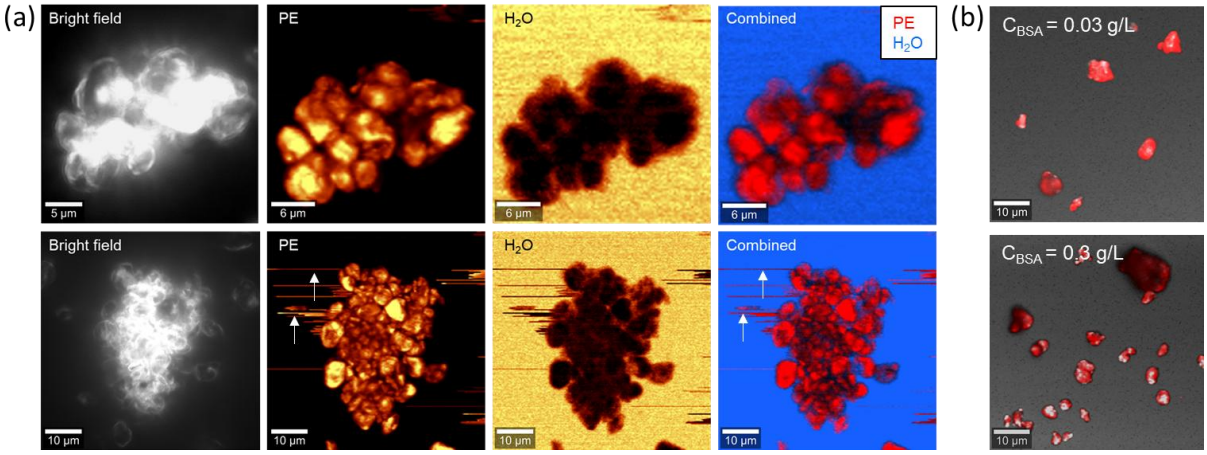

Fig. 9. *In situ* analysis of PE MPs agglomerates by Raman microscopy. (a) From left to right: bright field image, Raman image of PE, Raman image of H_2O, combined Raman image of PE (red) and H_2O (blue). A small and large agglomerate are shown for the same concentration C(BSA) = 0.3 g/L. Scale bar 6 µm (top) and 10 µm (bottom). White arrows indicate the binding or detachment of particles to/from the agglomerate during scanning. (b) Raman images of PE (red) from dry deposits on Si wafers from PE suspensions with C(BSA) = 0.03 g/L (top) and 0.3 g/L (bottom). Scale bar 10 µm.

The size of the primary particles in the agglomerate can be estimated after segmentation of the Raman image of PE (Fig. S13) and compared to the diameter of single PE particles from the dry deposits (Fig. 9b). The size analysis was not performed on single particles in suspension due to Brownian motion that impairs Raman imaging. The size analysis of the primary particles in the agglomerates *in situ* compared to particles from dry deposits confirmed that the agglomerates are composed of primary particles of the same size, excluding the trapping of smaller or larger MPs in the agglomerates.

3.6. Identification of secondary nanoplastics released during ageing

The analysis of PE MP suspensions by SEM revealed the presence of nanoplastics (d < 1 µm) in suspensions aged for 7 days without agitation (Fig. 10). Particles with irregular shapes and a diameter between 200 and 500 nm were clearly identified for C(BSA) ≥ 0.03 g/L. The fraction of nanoplastics is significant and could be underestimated due to the loss and/or the agglomeration of the smallest particles during deposition. By contrast, no nanoplastics were observed in fresh suspensions or in PP MP suspensions aged under the same conditions. Our results clearly suggest that the ageing of PE MPs with an excess of BSA can lead to the release of nanoplastics debris. BSA acts as a surfactant and can favor the dissociation of nanoplastics through the reorganization of the polymer chains, followed by the stabilization of the released particles in suspension by fast protein adsorption that increases the

surface hydrophilicity and charge. The difference in the behavior of PP and PE particles may be related to the polycrystalline nature of PE chains that forms subdomains within each particle [37].

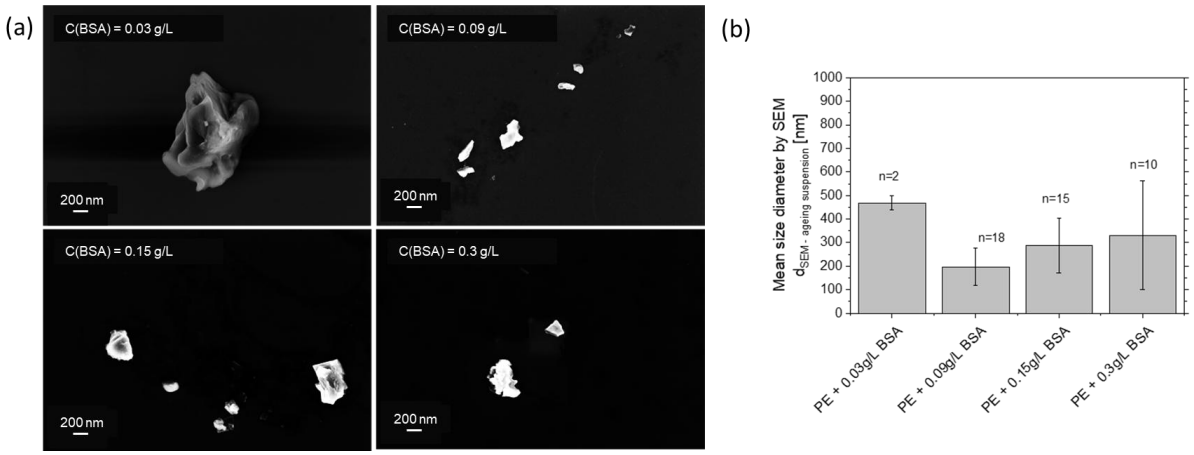

Fig. 10. Identification of nanoplastics from PE MP suspensions by SEM after ageing of the suspensions for 7 days in BSA solution. (a) SEM images and (b) size analysis of PE nanoplastics as a function of BSA concentration. A total number n = 45 nanoplastic particles were analyzed. Scale bar 200 nm.

These observations confirm that SEM is a method of choice for the dimensional size characterization of micro- and nano-plastics and provides evidence of the influence of the corona on the release of nanoplastic debris from soft polymeric microparticles in suspension.

4. Discussion

4.1. Influence of the corona on the dimensional analysis of MPs

The analysis of MP suspensions is not possible without a biocorona because the MPs do not mix or enter the aqueous solution due to their high hydrophobicity. Indeed, no particles were detected in the suspension without BSA. The deposition of micro or nanoplastics on SEM substrate for single particle analysis also requires the stabilization of MPs in suspension. Similarly, the measurement of MP density by SAXS is not possible on the dry powder.

The adsorption of BSA on nanomaterials has been widely studied in the literature, for example by Norde et al on silica nanoparticles [55], by Yoon et al and Baier et al on polystyrene microspheres [56, 57] to cite just a few examples. Depending on surface chemistry, surface charge, and particle size, both enthalpic (ΔH_{ads}) and entropic ($T.\Delta S_{ads}$) contributions can drive BSA adsorption through electrostatic interactions, hydrogen bonding, protein conformational changes (ΔH_{ads}), or hydrophobic interactions mediated by the desorption of water molecules ($T.\Delta S_{ads}$). Notably, the adsorption of negatively charged BSA on negatively charged particles, including functionalized polystyrene microspheres, was reported [57]. In this case, clusters of basic residues such as arginine may facilitate

electrostatic interactions and H bonding [58], while hydrophobic interactions predominate at low surface charge for functionalized polystyrene [56].

More recently, the adsorption of BSA on PVC MPs [59] and polyolefin MPs [37] was investigated by isothermal calorimetry (ITC), vibrational spectroscopy, and synchrotron-radiation deep UV fluorescence microscopy. The thermodynamic analysis showed that electrostatic interactions and conformation changes play a role in the adsorption of BSA on PVC [59]. Label-free imaging of adsorbed BSA by deep UV fluorescence microscopy showed that the protein quality, expressed in terms of surface coverage and homogeneity at a single particle level, was different between PE and PP MPs. BSA formed a more homogeneous and denser protein corona on PP MPs compared to PE [37]. This is in agreement with the higher amount of adsorbed BSA on PP MPs (1.5 ± 0.1 mg/m² for PE, 2.6 ± 0.2 mg/m² for PP) [37].

Based on the mass of adsorbed BSA, we can estimate the number of adsorbed molecules to 1.4 x 10^{16} and 2.4 x10^{16} molecules/m² for PE and PP MPs respectively. The hydrodynamic radius of BSA in pure water is 3.9 nm [60]. Assuming a spherical protein, the available surface for one BSA molecule within the protein corona can be estimated to 73 nm² on PE MPs and 42 nm² on PP MPs. By comparison, the average surface of one BSA molecule in water corresponds to 48 nm². This calculation confirms that BSA forms a fully packed corona on PP and a looser corona on PE MPs that can be evaluated to one and up to 2 layers of adsorbed proteins. It is in agreement with the study of Yoon et al, who calculated an adsorbed layer thickness of BSA on functionalized microspheres of 4.6 to 7.1 nm corresponding to a monolayer of side-on or end-on BSA molecules [56]. Thermodynamic analysis and simulations of protein adsorption [61] could provide information on the driving forces and molecular mechanisms of protein-MP interactions in future work.

In this study, we developed methodologies to characterize the dimensional size of PE and PP MPs with a BSA corona and investigate the effect of the protein corona on the size analysis of micro- and nano-plastic suspensions. The diameters of MPs in suspension d_{SEM}, d_{SMLS} and d_{Stokes} measured by SEM and SMLS using the density values determined by SAXS are compared in Fig. 11 and Fig. S14. The full data sets are presented in Table S2-S3. The diameters measured by SEM and SMLS (t = 0 s) are very similar, which suggests that suspensions are mostly composed of constitutive particles with few agglomerates. The increase of free BSA concentration in solution does not significantly change the average SEM and SMLS diameters of PE and PP MPs, suggesting that the initial stabilization of microplastics in suspension by the protein corona is not altered. At higher BSA concentrations, variability in size analysis between the different techniques is observed, suggesting differential behaviors and the onset of instability in the suspensions. While a complete corona is formed in all the conditions, these results suggest that the excess of free BSA may favor agglomeration, particle-particle interactions and dynamics in the suspension, a process in which a transient, low affinity, soft protein corona may be involved [61]. It is worth noting that the dimensional analysis of MP suspensions also

provides the opportunity to measure density through its integration with specific surface measurements, such as SAXS. The density of PE MPs in suspension was measured by combining SEM to determine the average particle diameter and SAXS to determine the Porod's limit of the particles.

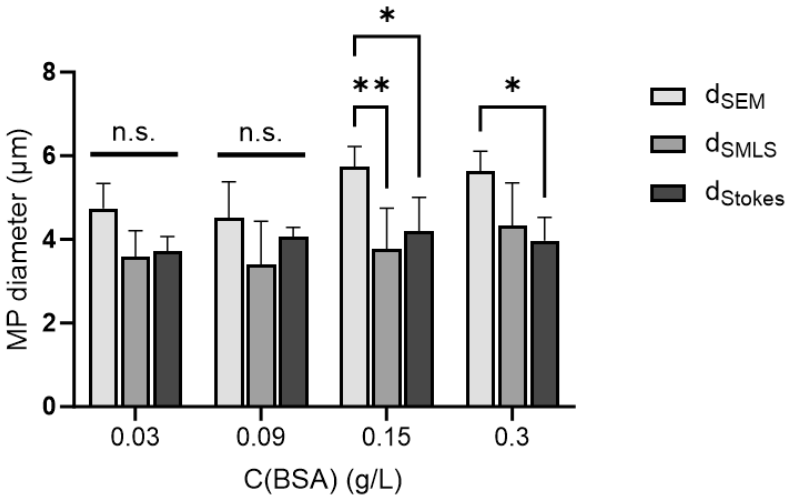

Fig. 11. Comparison of SEM, SMLS, and Stokes diameters of PE MPs measured in the experimental medium as a function of BSA concentration (n = 3) * $p < 0.05$, n.s. non-significant.

In toxicological studies, stability and dispersibility of MPs are key parameters that govern the exposure of cells in vitro and organisms in vivo. The number and size of particles that come into contact with cells/organisms depend on the creaming or sedimentation, and aggregation or fragmentation during exposure. The control of MP stability and dispersibility in suspension by BSA combined with their dimensional characterization provides a useful framework to evaluate the dose of exposure. Note that this study was performed at 20°C with purified BSA. The same methodology could be applied to the study of the size, stability, and dispersibility of various types of MPs in other media at lower or higher temperature.

4.2. Release of secondary nanoplastics and potential consequences

In the recent report *'Nanoplastics – State of knowledge and environmental and human health impacts'* mandated by the European Commission [62], the occurrence and the formation of secondary nanoplastics were discussed. Environmental studies revealed the presence of nano-sized (< 1 µm) plastics debris generated from secondary sources in the atmosphere and in aquatic environments [63, 64]. The identified sources of secondary nanoplastics are physical abrasion [64], degradation processes, and ageing [65]. Nowack et al showed that textiles are a significant source of nanoplastics released by abrasion during washing [66]. The release of nanoplastic debris by the ageing of PE MPs in suspension identified in this study reminds us that PE and PP are indeed called plastics because of their mechanical plasticity. This property originates from the mobility of the polymeric chains inside

the material. As a consequence, MPs are dynamic materials that are prone to evolution under mechanical, thermal, or chemical stress. The observation of secondary nanoplastics formed in aged suspensions without heating, photodegradation, or mechanical stress suggests that an equilibrium between a high and a low specific surface area form of the same material is observed here. According to this model, the excess of BSA would shift the equilibrium towards the high specific surface area form. Thus, the fraction released from plastics through erosion of their surfaces produce fragments of microplastics (d > 1 µm), but also particles smaller than 1 µm in size, which we define here as nanoplastics (d = 1 nm - 1µm). To date, the characterization of nanoplastics remains challenging. The number of nanoplastic fragments increased with increasing exposure time of MPs in BSA media **without mechanical stress** (Fig. 10b**)**. A variety of plastic fragment sizes, morphologies and shapes were found in our experiments. Debris released in the suspension could be described as small and irregular fragments and cracked particles (Fig. 12b**)**. PE MPs produced a higher number of small fragments including nanoplastics (200 – 500 nm) compared to PP MPs under the same experimental conditions. Our observations detailed in this study reveal the potential release of nanoplastics if we consider a size threshold of 1 µm for this type of nanomaterial. The release of nanoplastics could result from a continuous mechanism in spatiotemporally dynamic media with specific physico-chemical properties, including ionic strength gradients [67, 68]. Bonacci et al suggested that solid-solid contacts play a role in the ageing mechanisms of dense colloidal suspensions at rest [69]. This contact-controlled ageing may concern a whole range of materials, including MPs.

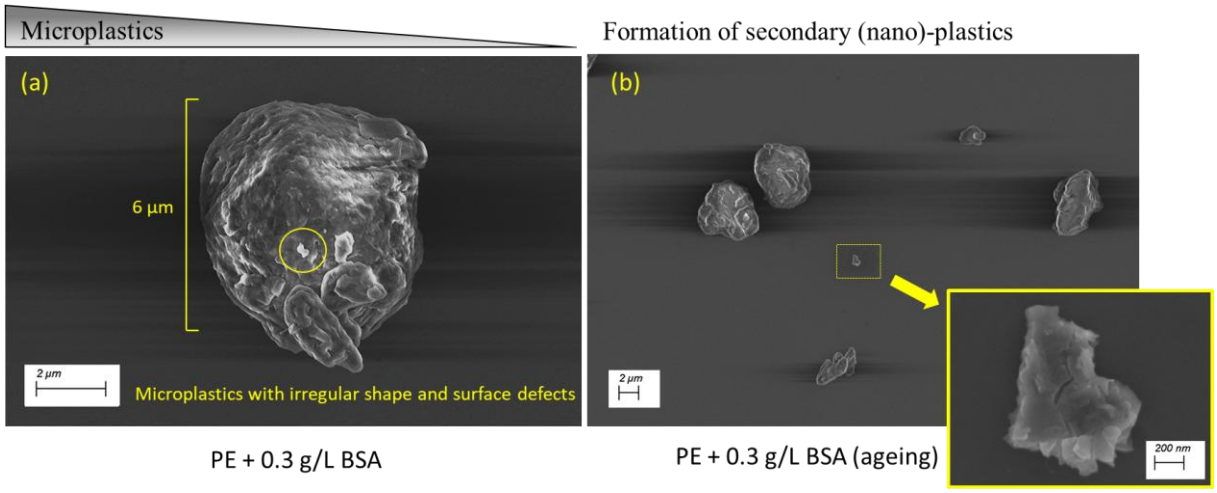

Fig. 12. Illustration of the release of secondary (nano)-plastics after ageing in BSA solution: (a) PE MPs before ageing showing irregular shapes and surface defects, (b) PE MPs and NPs after ageing.

The release of nanoplastics is also critical in terms of pollution as an increase in specific surface area may favor the release of toxic additives or the adsorption of toxic contaminants such as perfluoroalkyls (PFAS) [70]. As nanoplastics are stabilized by a corona, the sorption of contaminants will also depend on the exchange between adsorbed proteins and free contaminants that directly depends on the affinity of the contaminant for the surface and the concentration of the contaminant in

the environment. As proteins are adsorbed in a non-covalent way with a moderate affinity, the exchange of small hydrophobic pollutants, such as bisphenols or perfluoroalkyls, which could further enter the polymeric structure by diffusion, may occur.

Compared to extensive studies on abiotic mechanisms, few occurrences of MP fragmentation by biotic processes have been reported. Yet, the fragmentation of ingested MPs into nanoplastics was evidenced in aquatic organisms, such as in the Antarctic krill *Euphausia superba* [71] and in the freshwater amphipod *Gammarus duebeni* [72] that were able to rapidly fragment PE MPs. The formation of a biocorona has also been shown to favour particle size reduction through dissolution of cobalt nanoparticles in biological media [73]. We further demonstrated in this study that nanoplastic debris were formed in PE MP suspensions without mechanical stress, a process that is favoured by the formation of a biocorona on MPs. Together, these results suggest that biotic processes that are not limited to specific enzymatic degradation of synthetic polymers may play a crucial and understudied role in the fate of MPs in organisms.

4.3. Methodologies for the metrology of MP suspensions

Despite the identification of many emerging sources of nanoplastics in the environment, there is a gap between the ability to sample, isolate, detect nanoplastics on one hand, and the possibility to characterize and quantify nanoplastics on the other hand [22, 74]. Nanoplastics size is below the instrumental limit of detection of infrared spectroscopy and coherent Raman microscopy. For this reason, few studies have provided images of nanoplastics. It is therefore crucial to explore new methodologies to analyze nanoplastics.

SEM, TEM, FTIR and Raman microscopy, and to a lesser extent fluorescence microscopy, have been used for the identification and size measurement of microplastics [62]. Quian et al recently demonstrated the detection and identification of nanoplastics using Stimulated Raman Scattering [75]. This approach has significantly lifted the limitation of Raman microscopy in terms of spatial resolution and sensitivity for the detection of nanoplastics. DLS (Dynamic Light Scattering) is the reference method for the study of nanoparticles stability in suspension, although the size range of the instrument and the low stability of MPs in aqueous suspensions make it more difficult to apply to MPs compared to manufactured nanomaterials [74]. In this study, we developed the analysis of MP size and stability using SMLS and the analysis of MP density in suspension by SAXS. Lee et al used SMLS to monitor the sedimentation of polystyrene microspheres in methanol during synthesis [76]. This technique was also used to study the aggregation of core-shell polystyrene-iron oxide nanoparticles in Pickering emulsions by Han et al [77]. There are few reports on the analysis of other types of MPs by SMLS to our knowledge. Even if SEM is common for imaging MPs, the European Commission report on nanoplastics [62] underlined the current limitations of SEM analysis due to quantification difficulties, sample preparation, and charging effect. We solved these problems by improving sample deposition on silicon wafers and preventing charging effects by flowing nitrogen gas near the surface

to neutralize the charge effect. Using this method, we successfully measured nanoplastics size by SEM with high spatial resolution. The PE and PP MPs chosen in this study have a spherical shape, even if they are not perfect spheres (such as polystyrene microspheres). It would be interesting to extend the dimensional analysis of MPs by SEM to MP fibres to characterize the release of synthetic textile fibres of various lengths and diameters in the environment [78].

Despite the formation of a protein corona on PP MPs, the fast creaming rate of the particles and the lower stability of the suspensions prevented the accurate measurement of PP density by SAXS. We also observed differences between replicates that suggests that instability was triggered by other mechanisms. Future work could further investigate the molecular mechanisms that drive such instability, depending on the exposure medium and experimental conditions.

4.4. Towards a unified definition of nanoplastics

Plastic pollution takes three forms, depending on the size of the pieces of plastic found in the environment. These are macroplastics, microplastics, and nanoplastics. Various definitions are employed to conceptualize the presence of micro/nanoplastics and debris in marine, freshwater, sludge and environmental ecosystems as well as in food or drinking water. Significant differences exist in the definition on size. The lack of global standardization of nomenclature, harmonization of test methods for dimensional characterization, and reference materials complicates the situation. The ‘grey’ area regarding the class boundary between micro and nanoplastics is undoubtedly due to the high level of equipment required to observe nanoplastics. Collaboration between research teams, involving nanoplastics specialists, could provide an initial solution.

It is necessary to employ multiple methods for detection and characterization, and methods available to date for micro and nanoplastics may not be appropriate to detect and quantify nanoplastics [22, 35, 74]. Moreover, standardization of size class limits is needed to facilitate the exchange of results between teams, enabling comparisons that will facilitate the understanding of the phenomena. SEM is a method of choice that provides data on nanoplastic morphology, information that is still missing. Additionally, this method can be combined with chemical analysis strategies by EDX (Energy-Dispersive X-ray spectroscopy) and EBSD (Electron Backscatter Diffraction) [26].

5. Conclusions

Using SEM, SMLS, SAXS, and Raman microscopy, we developed methodologies for the dimensional size analysis and the physicochemical characterization of PE and PP MPs with a BSA corona in suspension. We completed the dimensional characterization of microplastics stabilized by a protein corona, including the measurement of Stokes diameter and particle density. The analysis of the effect of the biocorona on the dimensional characterization of MPs revealed that ageing of MPs in suspensions resulted in the release of secondary nanoplastics. SEM can be used for *ex situ* dimensional analysis of micro- and nano-plastics, with the advantage of existing normalized methods for particle

analysis, where it showed good agreement with size analysis of suspensions by SMLS. MP density could be determined in suspension with high sensitivity by SEM combined with SAXS to determine the particle diameter and Porod's limits respectively. Moreover, SEM was successfully applied to the detection of nanoplastic fractions that would have been obscured by other methods due to the small fraction of nanoplastics. The identification of nanoplastic debris in MP suspensions suggests that an excess of BSA favors the release of nanoplastics with a high specific surface area, potentially posing an additional threat to ecosystems. This observation strongly supports the adoption of a unified definition of nanoplastics and the inclusion of nanoplastics with a maximum size threshold of 1 µm in future regulations. In addition to SEM, we can also foresee the possible use of EDX and EBSD for their characterization.

Declaration of Competing Interest

The authors declare no competing interest.

Data availability

The datasets produced in this study are available from the corresponding authors upon request.

Acknowledgements

This work received state support managed by the French National Research Agency (ANR) under the France 2030 framework (FastNano, ANR-22-PEXD-0006). The authors acknowledge the Raman-AFM Platform (MPQ, Université Paris Cité) funded by ANR-18-IDEX-0001, IdEx Université Paris Cité. This project has received funding from the European Union's Horizon 2020 Research and Innovation Program under the grant agreement No. 965367 (PlasticsFate).

References

1. Stegmann, P., et al., *Plastic futures and their CO2 emissions.* Nature, 2022. **612**(7939): p. 272-276.
2. Babaremu, K.O., et al., *Sustainable plastic waste management in a circular economy.* Heliyon, 2022. **8**(7): p. e09984.
3. MacLeod, M., et al., *The global threat from plastic pollution.* Science, 2021. **373**(6550): p. 61-65.
4. Carpenter, E.J., et al., *Polystyrene Spherules in Coastal Waters.* Science, 1972. **178**(4062): p. 749-750.
5. Carpenter, E.J. and K.L. Smith, *Plastics on the Sargasso Sea Surface.* Science, 1972. **175**(4027): p. 1240-1241.
6. Venrick, E.L., et al., *Man-made Objects on the Surface of the Central North Pacific Ocean.* Nature, 1973. **241**(5387): p. 271-271.
7. Eriksen, M., et al., *Plastic Pollution in the World's Oceans: More than 5 Trillion Plastic Pieces Weighing over 250,000 Tons Afloat at Sea.* PLOS ONE, 2014. **9**(12): p. e111913.
8. Erni-Cassola, G., et al., *Distribution of plastic polymer types in the marine environment; A meta-analysis.* J Hazard Mater, 2019. **369**: p. 691-698.
9. Kooi, M., et al., *Ups and Downs in the Ocean: Effects of Biofouling on Vertical Transport of Microplastics.* Environmental Science & Technology, 2017. **51**(14): p. 7963-7971.

10. Reisser, J., et al., *The vertical distribution of buoyant plastics at sea: an observational study in the North Atlantic Gyre.* Biogeosciences, 2015. **12**(4): p. 1249-1256.
11. Tanaka, K. and H. Takada, *Microplastic fragments and microbeads in digestive tracts of planktivorous fish from urban coastal waters.* Scientific Reports, 2016. **6**(1): p. 34351.
12. Zhang, Y., et al., *Importance of atmospheric transport for microplastics deposited in remote areas.* Environmental Pollution, 2019. **254**: p. 112953.
13. Ross, P.S., et al., *Pervasive distribution of polyester fibres in the Arctic Ocean is driven by Atlantic inputs.* Nature Communications, 2021. **12**(1): p. 106.
14. Bhagat, K., et al., *Aging of microplastics increases their adsorption affinity towards organic contaminants.* Chemosphere, 2022. **298**: p. 134238.
15. Leslie, H.A., et al., *Discovery and quantification of plastic particle pollution in human blood.* Environment International, 2022. **163**: p. 107199.
16. Ragusa, A., et al., *Plasticenta: First evidence of microplastics in human placenta.* Environment International, 2021. **146**: p. 106274.
17. EFSA CONTAM Panel, *Presence of microplastics and nanoplastics in food, with particular focus on seafood.* EFSA Journal, 2016. **14**(6): p. e04501.
18. Commission, E., *COMMISSION REGULATION (EU) 2023/2055 of 25 September 2023 amending Annex XVII to Regulation (EC) No 1907/2006 of the European Parliament and of the Council concerning the Registration, Evaluation, Authorisation and Restriction of Chemicals (REACH) as regards synthetic polymer microparticles*, in *L 238/67*. 2023.
19. European Commission, *Annex XVII to Regulation (EC) No 1907/2006 of the European Parliament and of the Council concerning the Registration, Evaluation, Authorisation and Restriction of Chemicals (REACH) as regards synthetic polymer microparticles.* Official Journal, 2022.
20. Hernandez, L.M., et al., *Plastic Teabags Release Billions of Microparticles and Nanoparticles into Tea.* Environ Sci Technol, 2019. **53**(21): p. 12300-12310.
21. OECD, *Test No. 125: Nanomaterial Particle Size and Size Distribution of Nanomaterials*. 2022.
22. Caldwell, J., et al., *The micro-, submicron-, and nanoplastic hunt: A review of detection methods for plastic particles.* Chemosphere, 2022. **293**: p. 133514.
23. GESAMP, *Guidelines or the monitoring and assessment of plastic litter and microplastics in the ocean*, P.J. Kershaw, A. Turra, and F. Galgani, Editors. 2019. p. 130.
24. European Commission, *Commission Recommendation of 18 October 2011 on the definition of nanomaterial Text with EEA relevance.* Official Journal, 2011(275): p. 38-40.
25. European Commission, *Commission Recommendation of 10 June 2022 on the definition of nanomaterial C/2022/3689.* Official Journal, 2022.
26. Gigault, J., et al., *Current opinion: What is a nanoplastic?* Environ Pollut, 2018. **235**: p. 1030-1034.
27. Browne, M.A., T. Galloway, and R. Thompson, *Microplastic--an emerging contaminant of potential concern?* Integr Environ Assess Manag, 2007. **3**(4): p. 559-61.
28. Moore, C.J., *Synthetic polymers in the marine environment: A rapidly increasing, long-term threat.* Environmental Research, 2008. **108**(2): p. 131-139.
29. Ryan, P.G., et al., *Monitoring the abundance of plastic debris in the marine environment.* Royal Society, 2009. **354**(1526): p. 1999-2012.
30. Costa, M.F., et al., *On the importance of size of plastic fragments and pellets on the strandline: a snapshot of a Brazilian beach.* Environ Monit Assess, 2010. **168**(1-4): p. 299-304.
31. Desforges, J.P., et al., *Widespread distribution of microplastics in subsurface seawater in the NE Pacific Ocean.* Mar Pollut Bull, 2014. **79**(1-2): p. 94-9.
32. Wagner, M., et al., *Microplastics in freshwater ecosystems: what we know and what we need to know.* Environmental Sciences Europe, 2014. **26**(1): p. 12.
33. Koelmans, A.A., et al., *Microplastic as a Vector for Chemicals in the Aquatic Environment: Critical Review and Model-Supported Reinterpretation of Empirical Studies.* Environmental Science & Technology, 2016. **50**(7): p. 3315-3326.

34. Andrady, A.L., *Persistence of Plastic Litter in the Oceans*, in *Marine Anthropogenic Litter*, M. Bergmann, L. Gutow, and M. Klages, Editors. 2015, Springer International Publishing: Cham. p. 57-72.
35. Ivleva, N.P., A.C. Wiesheu, and R. Niessner, *Microplastic in Aquatic Ecosystems.* Angewandte Chemie International Edition, 2017. **56**(7): p. 1720-1739.
36. Martin, S., et al., *Pre-validation of a reporter gene assay for oxidative stress for the rapid screening of nanobiomaterials.* Frontiers in Toxicology, 2022. **4**.
37. Schvartz, M., et al., *Role of the Protein Corona in the Colloidal Behavior of Microplastics.* Langmuir, 2023. **39**(12): p. 4291-4303.
38. Fadare, O.O., et al., *Eco-Corona vs Protein Corona: Effects of Humic Substances on Corona Formation and Nanoplastic Particle Toxicity in Daphnia magna.* Environmental Science & Technology, 2020. **54**(13): p. 8001-8009.
39. Zhu, M., et al., *Eco-Corona Dictates Mobility of Nanoplastics in Saturated Porous Media: The Critical Role of Preferential Binding of Macromolecules.* Environmental Science & Technology, 2023. **57**(1): p. 331-339.
40. Cao, J., et al., *Coronas of micro/nano plastics: a key determinant in their risk assessments.* Particle and Fibre Toxicology, 2022. **19**(1): p. 55.
41. ISO, *Dispersibility of solid particles into a liquid (ISO/TS 22107:2021).* 2021: p. 22.
42. Tong, H., et al., *Occurrence and identification of microplastics in tap water from China.* Chemosphere, 2020. **252**: p. 126493.
43. Thi-Yen Le, T., et al., *On the equilibrium surface tension of aqueous protein solutions – Bovine serum albumin.* Journal of Molecular Liquids, 2022. **347**: p. 118305.
44. Nanogenotox, *Standard operating procedures for characterization of the selected manufactured nanomaterials types*, E. Commission, Editor. 2011. p. 80.
45. Sentis, M.P.L., et al., *Numerical prediction of long-term stability of liquid formulations determined by visual observation and static multiple light scattering.* Colloids and Surfaces A: Physicochemical and Engineering Aspects, 2023. **663**: p. 131070.
46. Foucher, J., et al., *The coming of age of the first hybrid metrology software platform dedicated to nanotechnologies (Conference Presentation)*. SPIE Advanced Lithography. Vol. 10145. 2017: SPIE.
47. Kirillov, A., et al., *Segment Anything.* arXiv, 2023. **2304.02643**.
48. Schindelin, J., et al., *Fiji: an open-source platform for biological-image analysis.* Nature Methods, 2012. **9**(7): p. 676-682.
49. Feigin, L.A. and D.I. Svergun, *Structure Analysis by Small-Angle X-Ray and Neutron Scattering*. 1987: Springer New York, NY.
50. Bouzakher-Ghomrasni, N., et al., *Dimensional measurement of TiO2 (Nano) particles by SAXS and SEM in powder form.* Talanta, 2021. **234**: p. 122619.
51. Hondow, N., et al., *STEM mode in the SEM: A practical tool for nanotoxicology.* Nanotoxicology, 2011. **5**(2): p. 215-227.
52. Roth, G.A., N.M. Neu-Baker, and S.A. Brenner, *SEM analysis of particle size during conventional treatment of CMP process wastewater.* Science of the Total Environment, 2015. **508**: p. 1-6.
53. Garcia-Diez, R., et al., *Simultaneous size and density determination of polymeric colloids by continuous contrast variation in small angle X-ray scattering.* European Polymer Journal, 2016. **81**: p. 641-649.
54. Garcia-Diez, R., C. Gollwitzer, and M. Krumrey, *Nanoparticle characterization by continuous contrast variation in small-angle X-ray scattering with a solvent density gradient.* Journal of Applied Crystallography, 2015. **48**: p. 20-28.
55. Giacomelli, C.E. and W. Norde, *The Adsorption–Desorption Cycle. Reversibility of the BSA–Silica System.* Journal of Colloid and Interface Science, 2001. **233**(2): p. 234-240.
56. Yoon, J.-Y., et al., *Adsorption of BSA on Highly Carboxylated Microspheres—Quantitative Effects of Surface Functional Groups and Interaction Forces.* Journal of Colloid and Interface Science, 1996. **177**(2): p. 613-620.

57. Baier, G., et al., *BSA Adsorption on Differently Charged Polystyrene Nanoparticles using Isothermal Titration Calorimetry and the Influence on Cellular Uptake.* Macromolecular Bioscience, 2011. **11**(5): p. 628-638.
58. Mathé, C., et al., *Structural Determinants for Protein adsorption/non-adsorption to Silica Surface*. PLOS ONE, 2013. **8**(11): p. e81346.
59. Ju, P., et al., *New insights into the toxic interactions of polyvinyl chloride microplastics with bovine serum albumin.* Environmental Science and Pollution Research, 2021. **28**(5): p. 5520-5531.
60. Zhang, X., et al., *Tracking structural transitions of bovine serum albumin in surfactant solutions by fluorescence correlation spectroscopy and fluorescence lifetime analysis.* Soft Matter, 2015. **11**(12): p. 2512-2518.
61. Sanchez-Guzman, D., et al., *In Situ Analysis of Weakly Bound Proteins Reveals Molecular Basis of Soft Corona Formation.* ACS Nano, 2020. **14**(7): p. 9073-9088.
62. European Commission, *Nanoplastics – State of knowledge and environmental and human health impacts*. 2023: Publications Office of the European Union.
63. Bianco, A. and M. Passananti, *Atmospheric Micro and Nanoplastics: An Enormous Microscopic Problem.* Sustainability, 2020. **12**(18): p. 7327.
64. Gangadoo, S., et al., *Nano-plastics and their analytical characterisation and fate in the marine environment: From source to sea.* Sci Total Environ, 2020. **732**: p. 138792.
65. Brewer, A., I. Dror, and B. Berkowitz, *The Mobility of Plastic Nanoparticles in Aqueous and Soil Environments: A Critical Review.* ACS ES&T Water, 2021. **1**(1): p. 48-57.
66. Yang, T., J. Luo, and B. Nowack, *Characterization of Nanoplastics, Fibrils, and Microplastics Released during Washing and Abrasion of Polyester Textiles.* Environmental Science & Technology, 2021. **55**(23): p. 15873-15881.
67. Cid-Samamed, A. and M.S. Diniz, *Recent Advances in the Aggregation Behavior of Nanoplastics in Aquatic Systems.* International Journal of Molecular Sciences, 2023. **24**(18): p. 13995.
68. Singh, N., et al., *Understanding the stability of nanoplastics in aqueous environments: effect of ionic strength, temperature, dissolved organic matter, clay, and heavy metals.* Environmental Science: Nano, 2019. **6**(10): p. 2968-2976.
69. Bonacci, F., et al., *Contact and macroscopic ageing in colloidal suspensions.* Nature Materials, 2020. **19**(7): p. 775-780.
70. Llorca, M., et al., *Adsorption of perfluoroalkyl substances on microplastics under environmental conditions.* Environmental Pollution, 2018. **235**: p. 680-691.
71. Dawson, A.L., et al., *Turning microplastics into nanoplastics through digestive fragmentation by Antarctic krill.* Nature Communications, 2018. **9**(1): p. 1001.
72. Mateos-Cárdenas, A., et al., *Rapid fragmentation of microplastics by the freshwater amphipod Gammarus duebeni (Lillj.).* Sci Rep, 2020. **10**(1): p. 12799.
73. Mei, N., et al., *Influence of Biocorona Formation on the Transformation and Dissolution of Cobalt Nanoparticles under Physiological Conditions.* ACS Omega, 2019. **4**(26): p. 21778-21791.
74. Caputo, F., et al., *Measuring particle size distribution and mass concentration of nanoplastics and microplastics: addressing some analytical challenges in the sub-micron size range.* Journal of Colloid and Interface Science, 2021. **588**: p. 401-417.
75. Qian, N., et al., *Rapid single-particle chemical imaging of nanoplastics by SRS microscopy.* Proceedings of the National Academy of Sciences, 2024. **121**(3): p. e2300582121.
76. Lee, J., et al., *Synthesis of highly monodisperse polystyrene microspheres via dispersion polymerization using an amphoteric initiator.* Journal of Colloid and Interface Science, 2006. **298**(2): p. 663-671.
77. Han, S., et al., *High-Performance Magnetorheological Suspensions of Pickering-Emulsion-Polymerized Polystyrene/Fe3O4 Particles with Enhanced Stability.* Langmuir, 2018. **34**(8): p. 2807-2814.
78. Wang, Z.-M., et al., *SEM/EDS and optical microscopy analyses of microplastics in ocean trawl and fish guts.* Science of The Total Environment, 2017. **603-604**: p. 616-626.

901